https://doi.org/10.1016/j.ceramint.2021.04.041

pH-dependent doping level and optical performance of antimony-doped tin oxide nanocrystals as nanofillers of spectrally selective coating for energy-efficient windows

Boxu Shen[1]*, Yuanhao Wang[2,]*, Lin Lu[1], Hongxing Yang[1]

1. Renewable Energy Research Group (RERG), Department of Building Services Engineering, The Hong Kong Polytechnic University, Kowloon, Hong Kong

2. SUSTech Engineering Innovation Center, School of Environmental Science and Engineering, Southern University of Science and Technology, Shenzhen, Guangdong 518055, China

*Corresponding author: Boxu Shen; Yuanhao Wang

E-mail addresses: boxushen.shen@connect.polyu.hk (B. Shen);

yuanhaowang@yahoo.com, wangyh2020@mail.sustech.edu.cn (Y. Wang)

Abstract

The optimal pH value of the titration endpoint remains uncertain for the synthesis of antimony-doped tin oxide by the co-precipitation method. In this study, the influence of the pH titration endpoint on doping level and optical performance was systematically studied. The phase composition, microstructure, the valence state of Sb ions and thermodynamic behaviors of antimony-doped tin oxide were comprehensively investigated. The UV-Vis-NIR transmittance spectra of ATO glass and SEM images of ATO coating were also studied. When the pH value of the titration endpoint was 6, the measured doping ratio of Sb was 10.81% which was close to the initial Sb doping level of 10%. In the meanwhile, the content of Sb^{5+} ions also reached the maximum value of 76.4%. Especially, the spectrally selective coating exhibited optimally spectral selectivity with the average visible light transmittance of 77.24% and the average near-infrared shielding ratio of 80.06% respectively. The results show that the doping level and optical properties of antimony-doped tin oxide certainly relied on the pH value of the titration endpoint. It is of great significance

to scale up the production of antimony-doped tin oxide with superior near-infrared shielding performance and promote its practical application in the field of energy-efficient glazing.

Keywords: pH value, antimony-doped tin oxide, doping level, near-infrared shielding performance, energy-efficient glazing, co-precipitation method

1. Introduction

Nearly 40 % of the total energy consumption has been used in buildings for developed countries [1]. It was reported that cooling loads accounted for about a fifth of total electricity used in residential buildings [2]. Especially, the buildings in Hong Kong can receive plenty of sunshine throughout the year, so the use of air-conditioning has caused huge power consumption, which increased from 48.8×103 TJ in 2017 to 50.6×103 TJ in 2018 [3]. Windows, the essential part of buildings, are regarded as a key factor in affecting the building energy loads, due to their pivotal function in transferring heat and light [4, 5]. Glazing materials are widely used in windows of modern buildings, providing daylight and outside view for occupants. As is well known, the invisible near-infrared (NIR) radiation (780–2500 nm) accounts for about half of the total solar energy, and ordinary glass is of high transmittance for the whole solar spectrum [6]. It is explicit that the development of energy-efficient glazing is conducive to the energy conservation of buildings [7].

The optical and thermal properties of the glass can be tailored to specific needs through the application of the thin layer based on spectrally selective materials. So far, the most commonly used spectrally selective materials involve silver and transparent conductive oxides. At present, silver-based Low-E glass is the most common type of energy-saving glazing in the current market. A typical Low-E coating usually consists of three layers, where the silver layer is placed between the

two dielectric layers. The two layers not only protect the silver layer from the ambient environment but also raise the transmittance in the visible region [8]. Therefore, the price of low-E glass is relatively higher due to the complex configuration and stringent fabrication process. Moreover, when the low-E glazing is used to retrofit the installed windows where most of the them are single-paned, the only feasible way is to replace the whole windows with low-E double-pane windows, which further increases the cost. However, the preparation of spectrally selective coating based on transparent conductive oxide (TCO) is a much more attractive way compared with low-E coating. Instead of replacing all the glass panes, the spectrally selective coating made of transparent conductive oxides can be utilized to the existing single-pane windows directly by various deposition techniques. The most commonly used transparent conductive oxide is tin-doped indium oxide (ITO) [9]. However, ITO can only exhibit strong heat-shielding performance in part of near-infrared wavelength ranging from 1500 nm to 2500 nm and there is still high near-infrared transmittance in the wavelength below 1500 nm [10, 11]. Besides, indium is not very abundant and is expensive. Antimony-doped tin oxide nanocrystals (ATO), a kind of relatively affordable TCO, have been regarded as a promising alternative due to its low cost and good stability. At present, the most widely used way for synthesizing ATO nanocrystals is the liquid-phase method, mainly including the co-precipitation method [12-16] and the solvothermal method [17-22]. The solvothermal method, despite showing the advantages of better control of the particle morphology and dispersibility, requires long reaction time and the extensive use of organic solvents (such as benzyl alcohol and toluene), which is not sufficient environmental-friendly. Besides, the output of the powder is limited by the size of the autoclave, which is hard to scale up the production. By contrast, the co-precipitation method is a more efficient way to prepare ATO nanocrystals, which is not time-

consuming and avoids the large consumption of organic solvents. In this method, $NH_3 \cdot H_2O$ was widely used as the precipitant for the formation of the tin/antimony hydroxide. However, few studies have been reported to discuss the effect of pH value for the reaction system on the antimony doping level and the optical performance of ATO nanocrystals.

In this study, ATO nanocrystals were prepared by the co-precipitation method using $NH_3 \cdot H_2O$ as the precipitant. The as-prepared nanocrystals were subsequently dispersed in the polyvinyl alcohol (PVA) solution to fabricate the spectrally selective coating on the ordinary glass. The effects of pH value of the reaction system on the antimony doping level and the optical performance of ATO nanocrystals were investigated by means of X-ray diffraction (XRD), X-ray photoelectron spectroscopy (XPS), inductively coupled plasma-optical emission spectroscopy (ICP-OES), transmission electron microscopy (TEM), and UV-Vis-NIR spectrometer. Besides, the near-infrared shielding performance of the spectrally selective coating was examined by a simulated experiment.

2. Experimental section

2.1 Materials

Tin chloride pentahydrate ($SnCl_4 \cdot 5H_2O$), antimony chloride ($SbCl_3$), ammonium hydroxide solution ($NH_3 \cdot H_2O$ 25%–28%), polyvinyl alcohol (PVA), absolute ethanol (C_2H_5OH) and deionized water (H_2O). All the chemical reagents are of analytical grade and used without further treatment.

2.2 Synthesis of ATO nanocrystals

The ATO nanocrystals were prepared by co-precipitation method using $SnCl_4 \cdot 5H_2O$ as Sn source and $SbCl_3$ as Sb source respectively. First, a certain amount of $SnCl_4 \cdot 5H_2O$ was added into the deionized water, then $SbCl_3$ was introduced into the aqueous solution of $SnCl_4 \cdot 5H_2O$ with a Sb/(Sb+Sn) molar ratio of 10%. Diluted $NH_3 \cdot H_2O$, the precipitant, was dropped into the precursor

solution at a constant speed to form the hydroxide precipitation. During this process, the titrition endpoint of pH value reached 4, 5, 6, 7, 8 corresponding to the ATO sample S1, S2, S3, S4, S5 respectively. The resultant solution was kept at 60 ℃ for 1 hour and then centrifugated three times with absolute ethanol. The obtained precipitation was dried at 80 ℃ for 2 hours and then polished into powders. The as-prepared powders were subsequently placed a tube furnace and sintered at 1000 ℃ for 4 hours to get the desired samples.

2.3 Preparation of ATO/PVA composite films

ATO/PVA composite films were prepared by a facile mixed method. PVA powder was used as film former. The typical fabrication steps of the composite films were as follows. Firstly, 4 g PVA powder was dissolved in 100 mL deionized water under 70 ℃ water bath to form a homogeneous PVA dispersion. Subsequently, a certain amount of the as-synthesized ATO nanocrystals were dispersed in the above PVA solution with vigorous stirring for 4 h. Finally, the blue dispersion product was sprayed on the quartz glass substrate to form composite films.

2.4 Characterization

The phase compositions of nanoparticles were examined by X-ray diffraction (XRD) with Cu Kα radiation. The morphologies and microstructures of the nanoparticles were obtained by transmission electron microscopy (TEM) with an energy dispersive spectrum (EDS) attachment. The binding energies of Sb 3d were obtained by X-ray photoelectron spectroscopy (XPS). The optical performance of the prepared samples was measured by an UV-vis-NIR spectrophotometer. The thermal behavior of the sample was determined by thermal gravimetric analyzer within a temperature range of 25 ℃ - 1000 ℃ with a heating rate of 10 ℃ per minute. Inductively Coupled Plasma-Optical Emission Spectroscopy (ICP-OES) was conducted on the iCAP 6500 Thermo

spectrometer.

3. Results and discussion

To confirm the phase composition, XRD measurements were conducted to the nanocrystals prepared in the precursor solution different pH value. Fig. 1 presents the XRD patterns of the as-synthesized nanocrystals with the pH value of 4, 5, 6, 7, 8 in the precursor solution corresponding to the sample S1, S2, S3, S4, S5 respectively. It can be observed that all the patterns agreed well with the standard pattern of cassiterite SnO_2 (JCPDS 41-1445) without the presence of other phases (such as Sb_2O_3, Sb_2O_5), indicating that antimony has been totally doped into the crystal structure of the nanocrystals. Besides, the diffraction peaks of all the patterns were narrow and sharp, implying that all the nanocrystals were of good crystallinity. The average crystallite size calculated by Scherrer formula [23] ($D = 0.89\lambda/[B\cos\theta]$, where D, λ, B, θ was the crystallite size, the wavelength of X-ray, the full width at half maximum of (110), the half of the scanning angle respectively) was about 36.1, 37.8, 25.9, 28.7 and 31.9 nm for S1, S2, S3, S4 and S5, respectively.

Fig. 2 shows the survey spectra of as-prepared powders with different pH level in the synthetic process. It can be seen that the elements of Sn, Sb, and O existed in the nanocrystals, implying that Sb element has been successfully doped into the crystal structure. Fig. 3a-e display the core-level XPS spectra of Sb $3d_{3/2}$ within the scope of 538-546 eV. It was reported that two valence state of Sb ions coexisted in the ATO nanocrystals. The Sb $3d_{3/2}$ curves shown in Fig. 3a-e were fitted into two peaks at 541.7 and 542.6 eV corresponding to Sb^{3+} and Sb^{5+} respectively [21, 24]. The optical properties of the as-synthesized ATO nanocrystals were significantly affected by its electrical capabilities [24]. Sb^{5+} ions serve as electron donors, forming a light donor level near the conduction band of tin oxide, but Sb^{3+} ions act as the electron acceptors. When the two valence states of Sb ions

coexist, the compensating effect is inevitable. The n-doping dominated by Sb^{5+} ions contributes to a higher concentration of free electrons, which can lead to stronger localized surface plasmon resonance (LSPR) [25]. Thus, a high ratio of Sb^{5+} ions is conducive to improve the near-infrared shielding performance of the nanocrystals. According to the valance distribution of Sb shown in Fig. 3f, when the pH value in the precursor solution was 6, the content of Sb^{5+} ions was the highest, accounting for 76.4% of the total amount of Sb atoms. When the pH value reached 7, the content of Sb^{5+} ions decreased to 70.8%. With the increase of pH value in the synthetic process, the ratio of Sb^{5+} ions showed an increasing trend and reached the maximum content when the pH value was 6. After that, the ratio of Sb^{5+} ions decreased to 30.1% when the pH value in the precursor solution was 8. The results indicate that pH value of 6 in the precursor solution contributes the most Sb^{5+} ions in ATO nanocrystals, which plays a significant impact on the optical performance.

To further investigate the effect of pH value on the doping level, the Sb content (Sb/[Sb + Sn]mol%) of the samples was measured by ICP-OES and the ICP-OES measurement provided the Sb content in the whole sample. The initial doping ratio of the Sb content was 10%. As shown in Table 1, the Sb content displayed a decreasing trend with the increase of the pH value. When the pH value reached 6, the Sb content attained minimum value of 11.6%, which was close to the initial doping value of 10%. In the meanwhile, the content of Sb^{5+} ions also reached the maximum value of 76.4%. Continuing to increase the pH value, the Sb content presented an increasing trend and reached 13.5 when the pH value was 8. A plausible explanation for the above results is the changing formation of the tin hydroxide. Tin hydroxide is a kind of amphoteric hydroxide which can react with alkaline substance to form salt and water. During the titration process, Sn^{4+} ions started to form the tin hydroxide. When the pH value attained 6, it can be inferred

that nearly all Sn^{4+} ions formed the tin hydroxide. With the increase of $NH_3 \cdot H_2O$ in the precursor solution, the mass of tin hydroxide began to reduce, but the Sb content stated to increase.

Fig. 4 shows the TG/DSC curves of the precursor precipitate with the pH endpoint of 6 after the titration process as a function of temperature. The mass of the precursor precipitate displayed a rapid decline from starting temperature to 150 ℃, which might be attributed to the evaporation of water and ethanol from the rinsing process. The precipitate demonstrated a gradual weight loss between 150℃ and 400℃, followed by a tardy weight loss above 400℃. The DSC curve illustrated a continuously endothermic trend from 400℃. This tendency corresponds well with the TG function and indicates that the precursor precipitate started to transform into ATO nanocrystals by gradual decomposition reaction of the tin hydroxide.

The detailed structural information was determined using transmission electron microscopy (TEM). Fig. 5 presents the TEM image, HR-TEM image, SAED pattern and EDS pattern of the as-synthesized ATO nanocrystals with the pH value of 6 in the titration process. In Fig. 5a, most of the as-prepared nanoparticles show a circular shape. Fig. 5b is the HR-TEM image of the selected area in Fig. 5a and the lattice spacing is 0.269 nm, which is determined as plane of (101). The as-synthesized sample was further confirmed by the SAED pattern displayed in Fig. 5c. The element composition is shown in Fig. 5d, indicating the existence of Sn, Sb and O element. Besides, the measured Sb content is about 0.1081 which is quite close to the initial doping value of 10%, indicating that almost all Sb ions have been doped into the crystal structure of SnO_2.

Fig. 6 presents the XRD pattern of the ATO composite coating prepared by dispersion of the ATO nanocrystals with PVA as the film-forming agent. It can be seen that the diffraction peaks of the spectrally selective coating can be well indexed to the characteristic peaks of the standard patterns

JCPDS 41-1445. The results indicate that the phase composition of the as-prepared coating consists of ATO nanocrystals. Fig. 7 presents the SEM images corresponding to the top view and cross section of ATO composite coating. As shown in Fig. 7a, the coating showed homogeneous appearance without obvious grain boundaries, indicating the existence of a large part of amorphous phase. In Fig. 7b, it is found the cross section of the composite coating and the glass substrate. The thickness of the coating was estimated to be in the range of 10 μm to 15 μm.

As shown in Fig. 8a, the schematic of transparent heat-shielding mechanism is presented, which is ascribed to its superior spectral selectivity. ATO nanocrystals demonstrate strong LSPR in the near-infrared band to shield the radiation transmittance. Besides, the radiation of ultraviolet can be shielded to a certain extent due to the intrinsic absorption of ATO as a n-type semiconductor. Fig. 8b shows the UV-Vis-NIR transmittance spectra of ATO glass and ordinary glass. It can be seen that the coated glass showed lower transmittance in the near-infrared wavelength range and maintain a relatively high visible transparency. For the purpose of evaluating the optical properties of the coatings, three parameters were proposed, including T_{Vis} (average transmittance of visible light, 380-780 nm), T_{NIR} (average transmittance of near-infrared light, 780-2500 nm) and S_{NIR} (average shielding ratio of near-infrared light region, 780-2500nm) [23, 26]. The corresponding values calculated by the transmittance spectra shown in Fig. 8b are displayed in Table 2. It can be seen that the T_{Vis} of ATO glass is only 10.65% lower than that of ordinary glass, but the S_{NIR} of ATO glass reaches 80.06% which is much higher than that of ordinary glass. The results indicate that the ATO glass presents superior near-infrared shielding performance than ordinary glass due to the existence of the spectrally selective ATO coating.

4. Conclusions

In this work, the effect of the pH titration endpoint on the doping level for ATO nanocrystals was systematically studied via chemical co-precipitation method. The phase composition, element composition, valence state of Sb ions, microstructure and thermal characteristics of ATO nanocrystals were comprehensively investigated. The UV-Vis-NIR transmittance spectra of ATO glass and SEM images of ATO coating were also studied. The results demonstrate that the doping level of ATO nanocrystals certainly relied on the pH value of the titration endpoint. When the pH value of the titration endpoint was 6, the measured doping ratio of Sb was 10.81% which is close to the initial Sb doping level of 10%. In addition, the pH value of titration endpoint also plays an important impact on the content of Sb^{5+} ions. The content of Sb^{5+} ions also reached the maximum value of 76.4% when the pH value was 6.

Declaration of competing interest

The authors declare that they have no known competing financial interests or personal relationships that could have appeared to influence the work reported in this paper.

Acknowledgements

This work was supported by the TCS project of the Hong Kong Innovation and Technology Fund (UIT/139) and Sola Green Technologies Limited. This work was also supported by the National Natural Science Foundation of China (Grant No. 61705258).

References

[1] Ke Y, Zhou C, Zhou Y, Wang S, Chan SH, Long Y. Emerging Thermal-Responsive Materials and Integrated Techniques Targeting the Energy-Efficient Smart Window Application. Advanced Functional Materials. 2018;28.

[2] Zhuang C, Shan K, Wang S. Coordinated demand-controlled ventilation strategy for energy-efficient

operation in multi-zone cleanroom air-conditioning systems. Building and Environment. 2021;191.

[3] Min Y, Chen Y, Yang H. Investigation on dynamic behaviour of condensation heat transfer in indirective evaporative cooler. Indoor and Built Environment. 2020.

[4] Garlisi C, Trepci E, Li X, Al Sakkaf R, Al-Ali K, Nogueira RP, et al. Multilayer thin film structures for multifunctional glass: Self-cleaning, antireflective and energy-saving properties. Applied Energy. 2020;264.

[5] Cuce E, Riffat SB. A state-of-the-art review on innovative glazing technologies. Renewable and Sustainable Energy Reviews. 2015;41:695-714.

[6] Ran S, Liu J, Shi F, Fan C, Chen B, Zhang H, et al. Greatly improved heat-shielding performance of KxWO3 by trace Pt doping for energy-saving window glass applications. Solar Energy Materials and Solar Cells. 2018;174:342-50.

[7] Xie N, Niu J, Wu T, Gao X, Fang Y, Zhang Z. Fabrication and characterization of CaCl2·6H2O composite phase change material in the presence of CsxWO3 nanoparticles. Solar Energy Materials and Solar Cells. 2019;200.

[8] Nezhad EH, Haratizadeh H, Kari BM. Influence of Ag mid-layer in the optical and thermal properties of ZnO/Ag/ZnO thin films on the glass used in Buildings as insulating glass unit (IGU). Ceramics International. 2019;45:9950-4.

[9] Shen B, Wang Y, Lu L, Yang H. Synthesis and characterization of Sb-doped SnO2 with high near-infrared shielding property for energy-efficient windows by a facile dual-titration co-precipitation method. Ceramics International. 2020;46:18518-25.

[10] Song X, Liu J, Shi F, Fan C, Ran S, Zhang H, et al. Facile fabrication of KmCsnWO3 with greatly improved near-infrared shielding efficiency based on W5+-induced small polaron and local surface

plasmon resonance (LSPR) modulation. Solar Energy Materials and Solar Cells. 2020;218.

[11] Qi S, Xiao X, Lu Y, Huan C, Zhan Y, Liu H, et al. A facile method to synthesize small-sized and superior crystalline Cs0.32WO3 nanoparticles for transparent NIR shielding coatings. CrystEngComm. 2019;21:3264-72.

[12] Kim D-W, Kim D-S, Kim Y-G, Kim Y-C, Oh S-G. Preparation of hard agglomerates free and weakly agglomerated antimony doped tin oxide (ATO) nanoparticles by coprecipitation reaction in methanol reaction medium. Materials Chemistry and Physics. 2006;97:452-7.

[13] Liu S, Jiang W, Liu C, Ding W, Chai W. Preparation and characterization of ATO nanoparticles by various coprecipitation. Journal of Materials Science: Materials in Electronics. 2012;24:594-600.

[14] Khorshidi B, Hosseini SA, Ma G, McGregor M, Sadrzadeh M. Novel nanocomposite polyethersulfone- antimony tin oxide membrane with enhanced thermal, electrical and antifouling properties. Polymer. 2019;163:48-56.

[15] Karki HP, Ojha DP, Joshi MK, Kim HJ. Effective reduction of p-nitrophenol by silver nanoparticle loaded on magnetic Fe3O4/ATO nano-composite. Applied Surface Science. 2018;435:599-608.

[16] Li Y, Wang J, Feng B, Duan K, Weng J. Synthesis and characterization of antimony-doped tin oxide (ATO) nanoparticles with high conductivity using a facile ammonia-diffusion co-precipitation method. Journal of Alloys and Compounds. 2015;634:37-42.

[17] Yu N, Peng C, Wang Z, Liu Z, Zhu B, Yi Z, et al. Dopant-dependent crystallization and photothermal effect of Sb-doped SnO2 nanoparticles as stable theranostic nanoagents for tumor ablation. Nanoscale. 2018;10:2542-54.

[18] Yang L, Huang J, Shi L, Cao L, Liu H, Liu Y, et al. Sb doped SnO2-decorated porous g-C3N4 nanosheet heterostructures with enhanced photocatalytic activities under visible light irradiation. Applied

Catalysis B: Environmental. 2018;221:670-80.

[19] Lee HY, Cai Y, Bi S, Liang YN, Song Y, Hu XM. A Dual-Responsive Nanocomposite toward Climate-Adaptable Solar Modulation for Energy-Saving Smart Windows. ACS Appl Mater Interfaces. 2017;9:6054-63.

[20] Abendroth T, Schumm B, Alajlan SA, Almogbel AM, Mäder G, Härtel P, et al. Optical and thermal properties of transparent infrared blocking antimony doped tin oxide thin films. Thin Solid Films. 2017;624:152-9.

[21] Li Y, Liu J, Liang J, Yu X, Li D. Tunable solar-heat shielding property of transparent films based on mesoporous Sb-doped SnO(2) microspheres. ACS Appl Mater Interfaces. 2015;7:6574-83.

[22] Wang M, Xu Y, Liu Y, Wu W, Xu S. Synthesis of Sb-doped SnO2 (ATO) hollow microspheres and its application in photo-thermal shielding coating. Progress in Organic Coatings. 2019;136.

[23] Cai L, Wu X, Gao Q, Fan Y. Effect of morphology on the near infrared shielding property and thermal performance of K0.3WO3 blue pigments for smart window applications. Dyes and Pigments. 2018;156:33-8.

[24] Peters K, Zeller P, Stefanic G, Skoromets V, Němec H, Kužel P, et al. Water-Dispersible Small Monodisperse Electrically Conducting Antimony Doped Tin Oxide Nanoparticles. Chemistry of Materials. 2015;27:1090-9.

[25] Xu JM, Li L, Wang S, Ding HL, Zhang YX, Li GH. Influence of Sb doping on the structural and optical properties of tin oxide nanocrystals. CrystEngComm. 2013;15.

[26] Zhao Z, Bai Y, Ning W, Fan J, Gu Z, Chang H, et al. Effect of surfactants on the performance of 3D morphology W18O49 by solvothermal synthesis. Applied Surface Science. 2019;471:537-44.

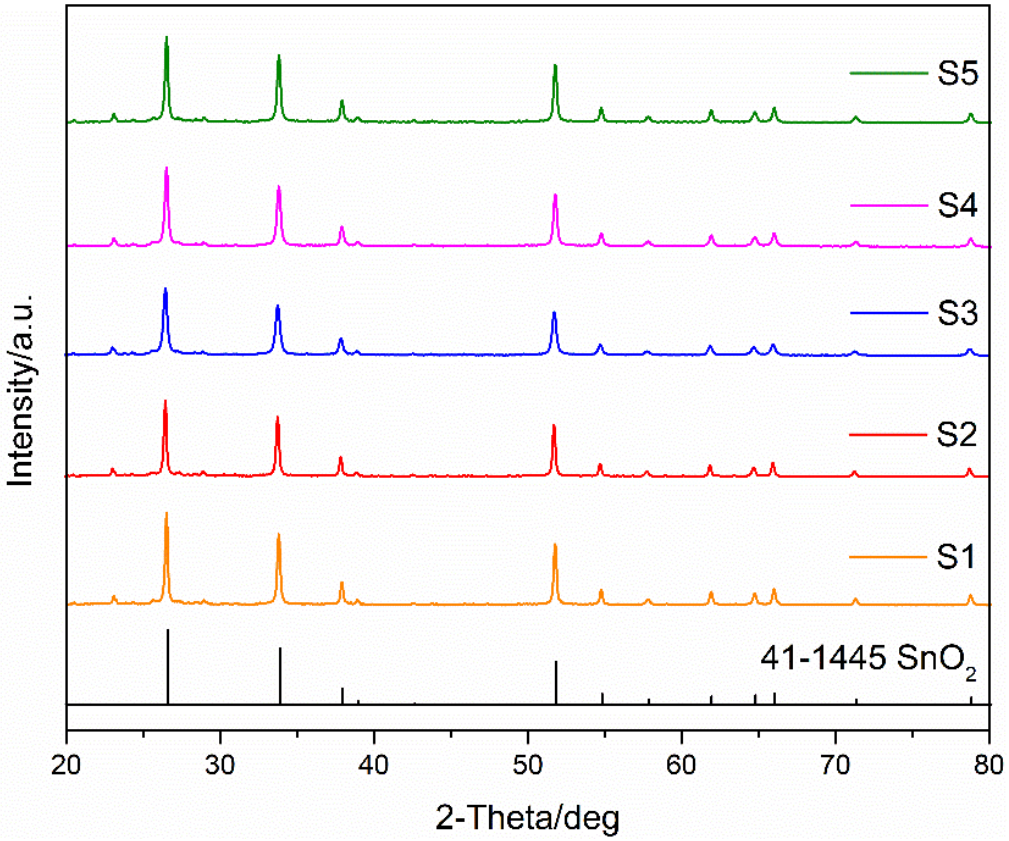

Fig. 1 XRD patterns of the powders prepared by different pH value in the precursor solution

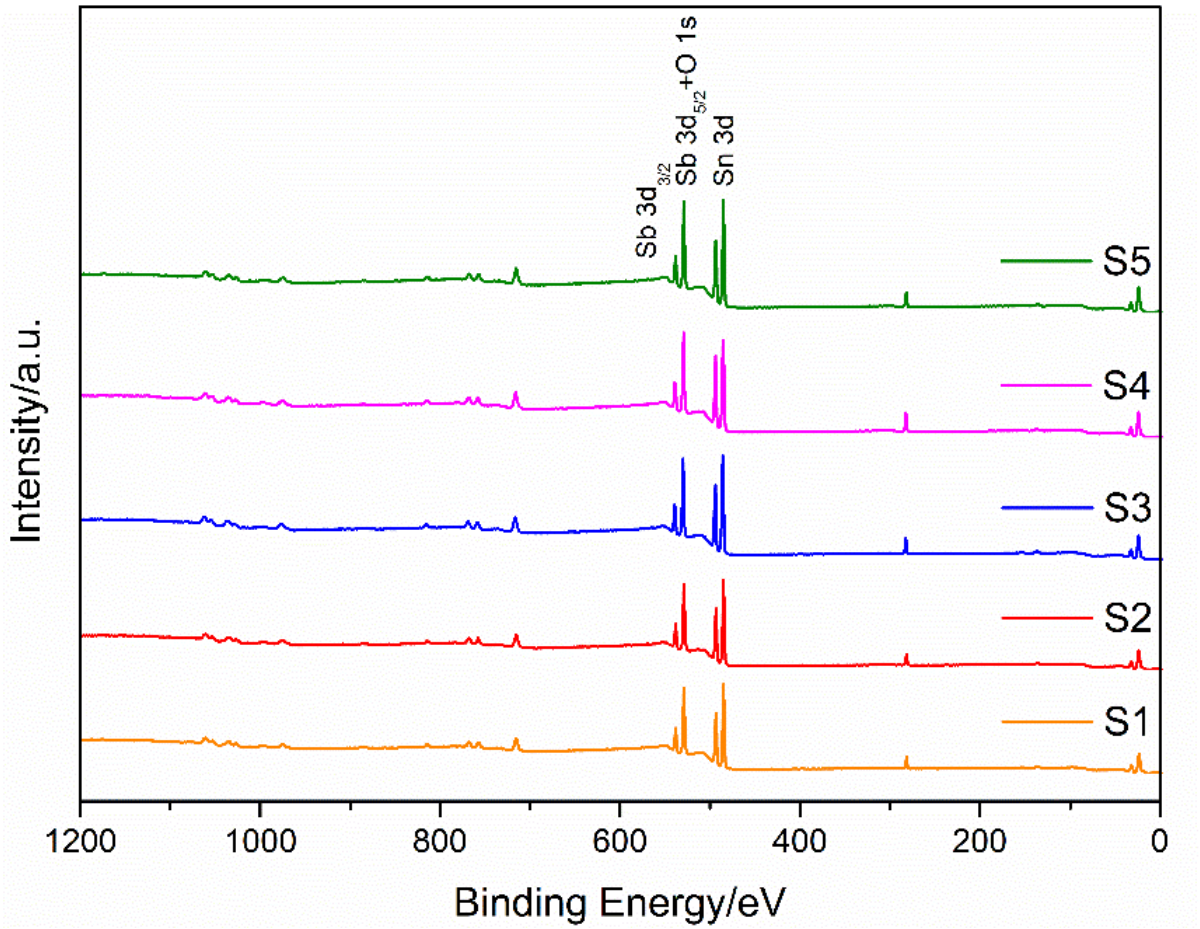

Fig. 2 Survey spectra of the powders with different pH value in the precursor solution

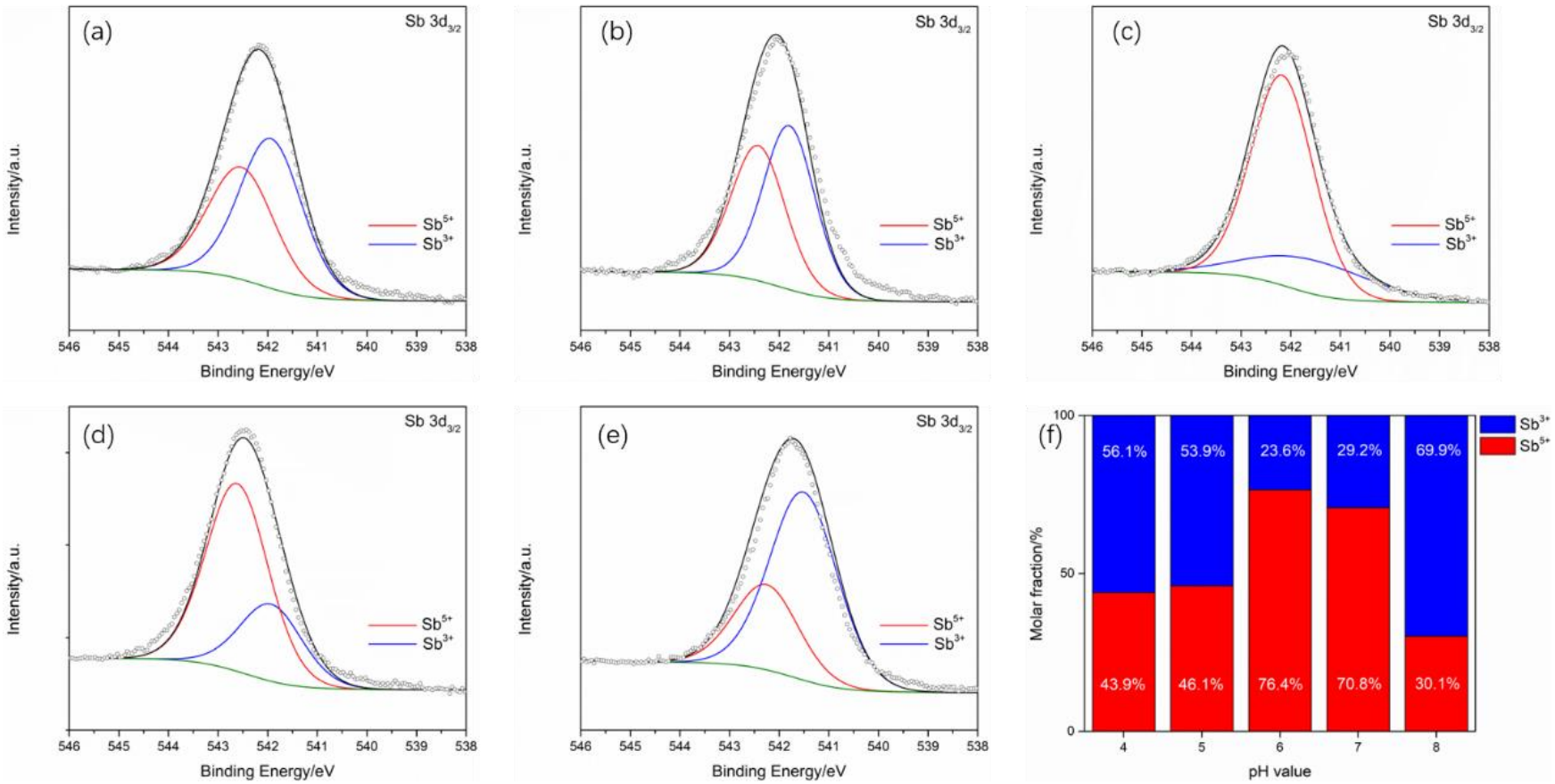

Fig. 3 (a)-(e) Sb $3d_{3/2}$ core-level spectra of ATO nanocrystals synthesized with different pH value in the precursor solution; (f) The valence distribution of Sb in ATO nanocrystals with different pH value in the precursor solution

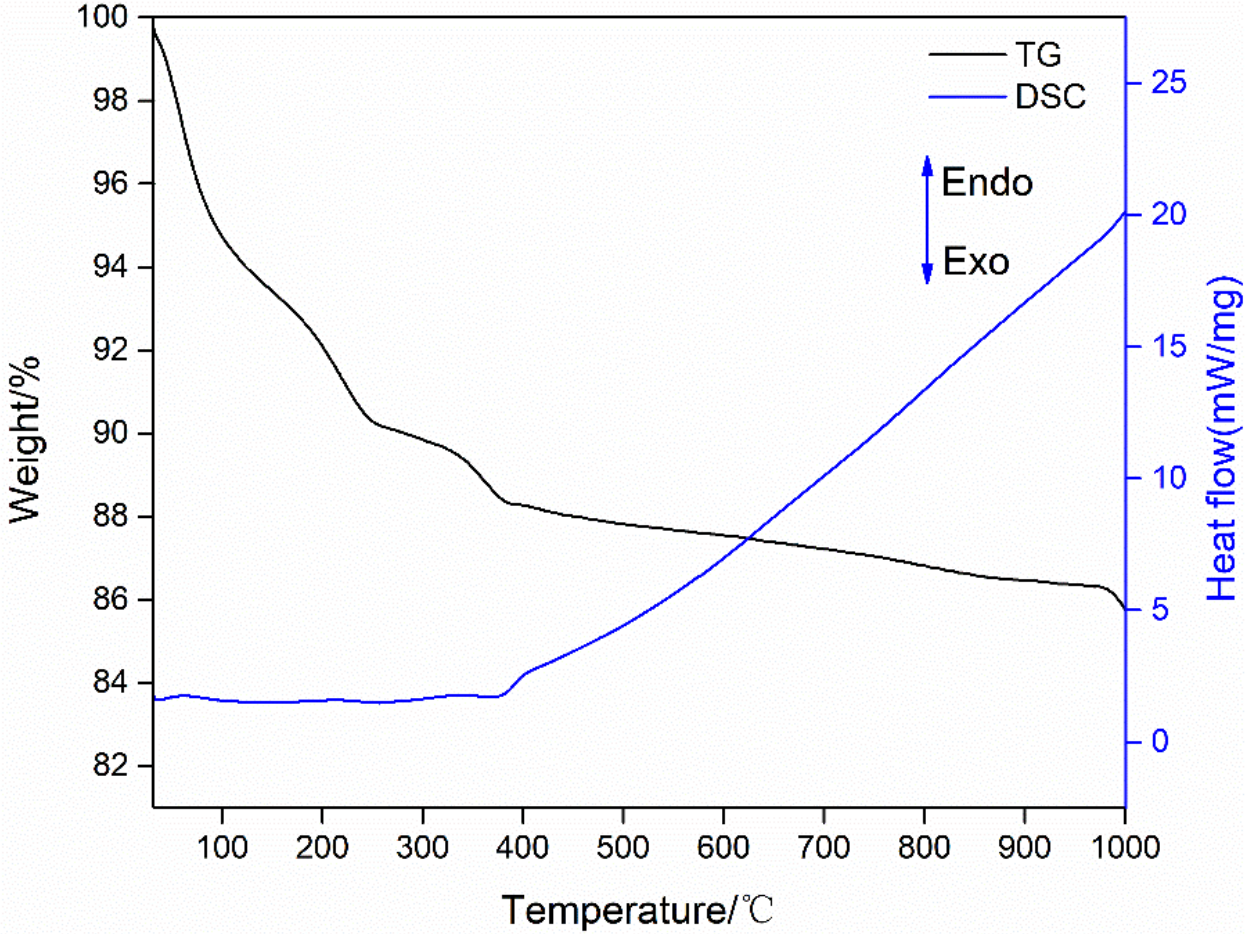

Fig. 4 TG/DSC curves of the precursor precipitate with the pH value of 6 in the synthetic process

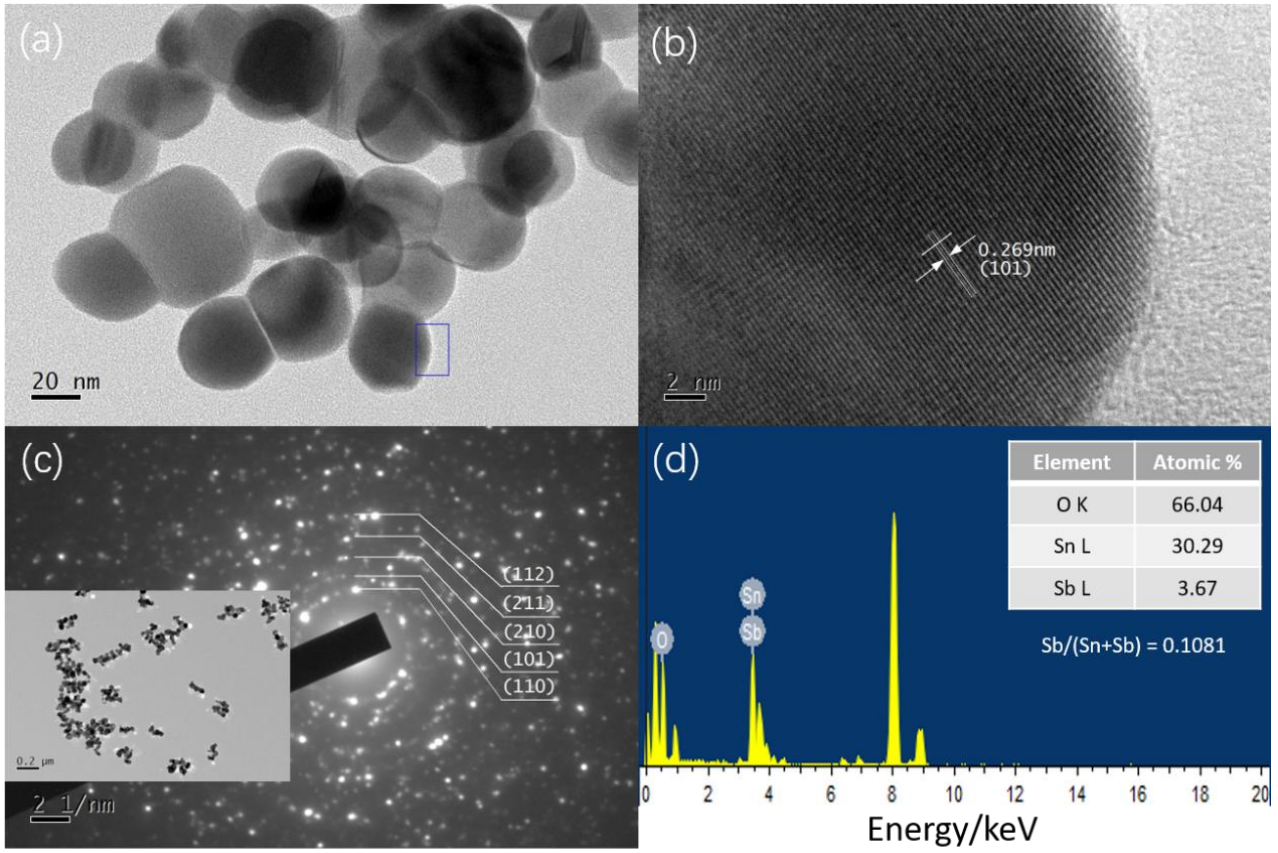

Fig. 5(a) TEM image of ATO nanocrystals with the pH value of 6, (b) HR-TEM image of the selected area, (c) SAED pattern of the inset area and (d) EDS pattern of the sample with the pH value of 6.

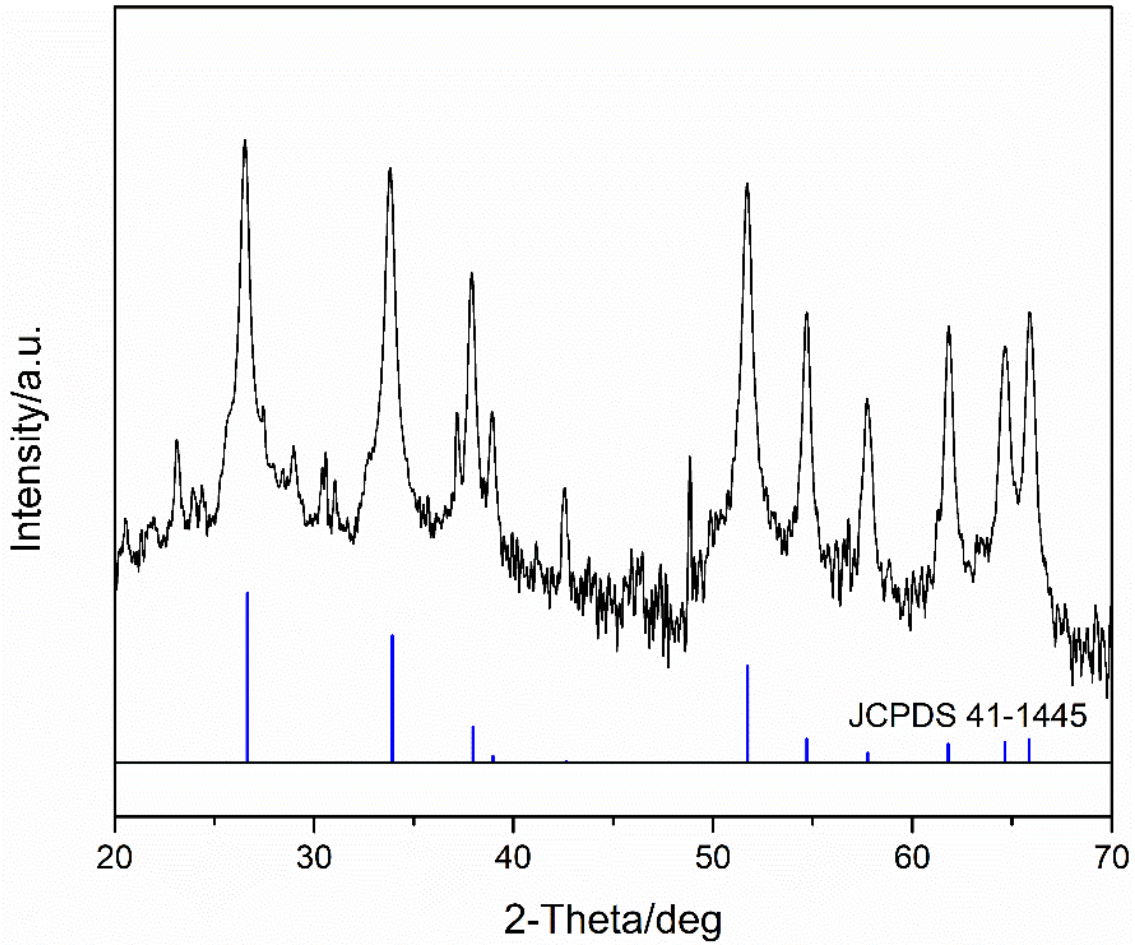

Fig. 6 XRD pattern of the ATO composite coating

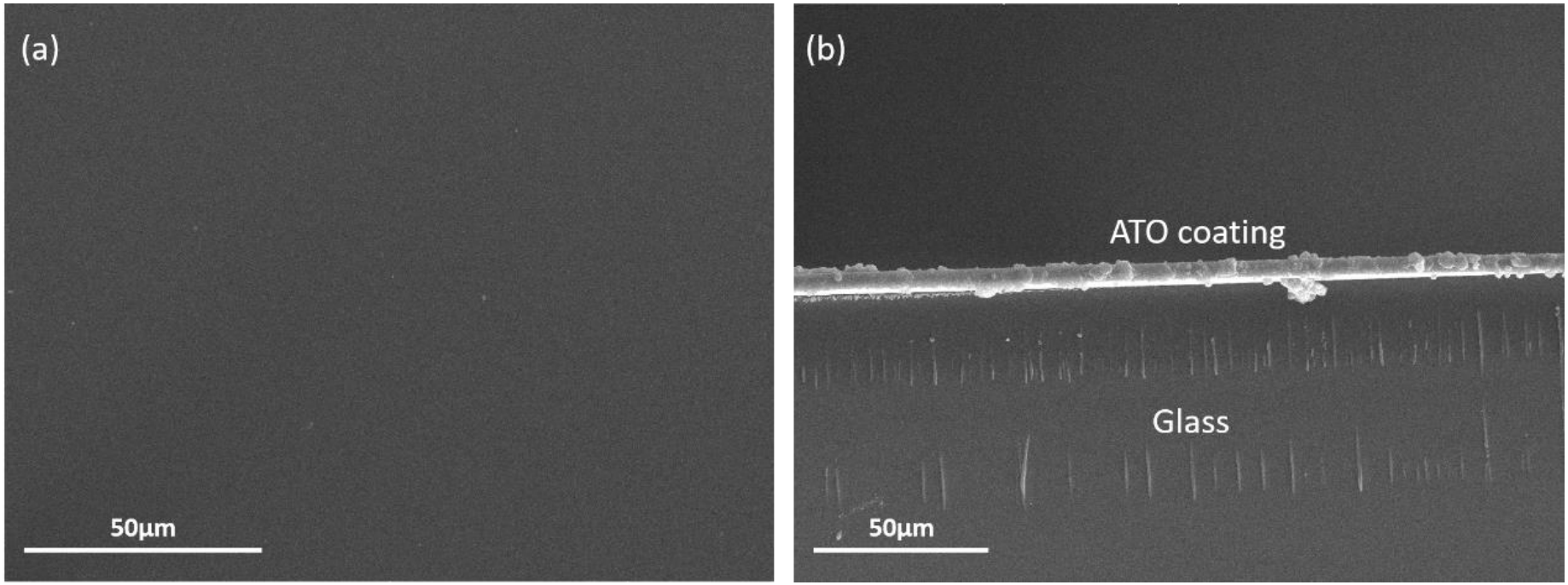

Fig. 7 SEM images of the (a) top view and (b) cross section of the ATO composite coating

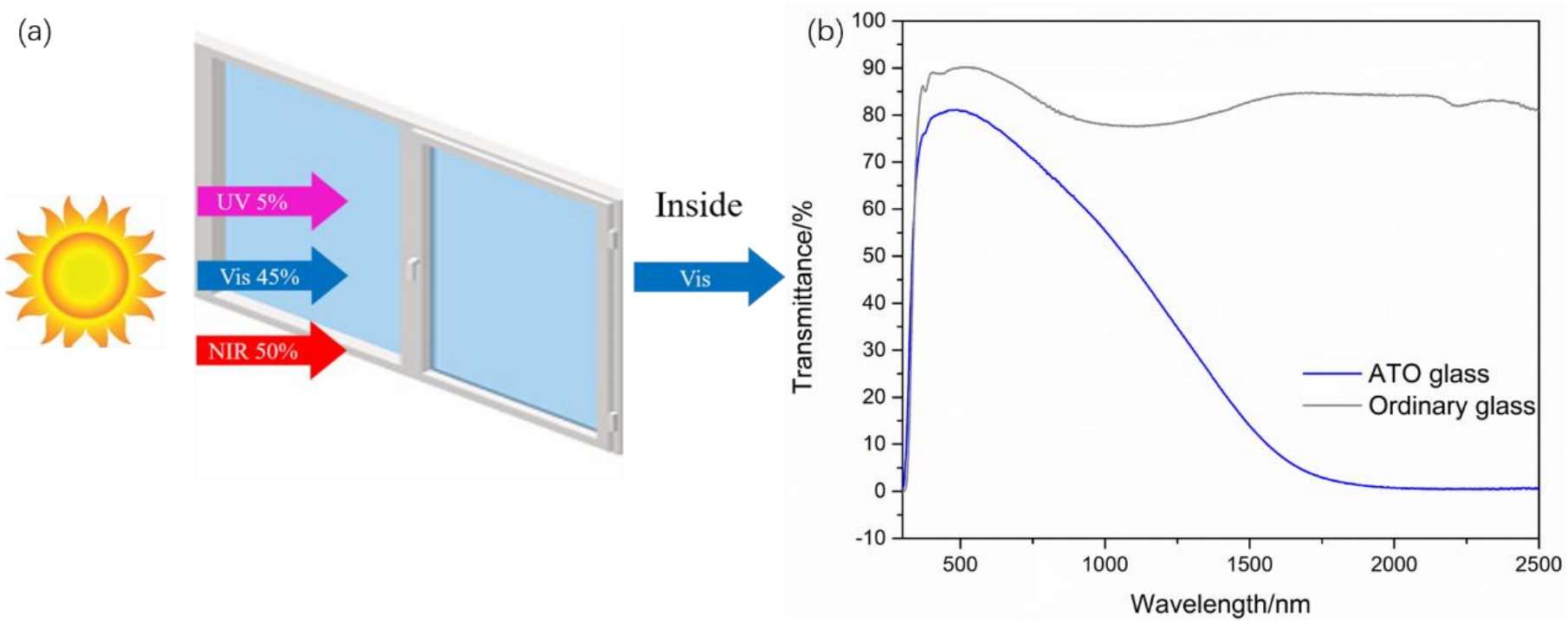

Fig. 8 (a) Diagram of the transparent heat-shielding mechanism for the glass with spectrally selective coating, (b) The UV-Vis-NIR transmittance spectra of ATO glass and ordinary glass

Table 1

The Sb content in ATO nanocrystals measured by ICP-OES and the molar fraction of Sb^{5+} in the two valence states

pH value	Sb content (mol %)	Sb^{5+}content (mol %)
4	22.8	43.9
5	13.8	46.1
6	11.6	76.4
7	12.9	70.8
8	13.5	30.1

Table 2

The optical parameters of the as-prepared ATO glass and ordinary glass

Sample	T_{Vis}[a] (%)	T_{NIR}[b] (%)	S_{NIR}[c] (%)
ATO glass	77.24	19.54	80.06
Ordinary glass	87.89	81.82	18.18

[a] Average transmittance of visible light region (380-780nm): $T_{vis} = \frac{\int_{380}^{780} T(\lambda) d(\lambda)}{(780-380)\times 100} \times 100\%$,

$T(\lambda)$ is the function curve of spectral transmittance with wavelength as independent variable

[b] Average transmittance of near-infrared light region (780-2500nm): $T_{NIR} = \frac{\int_{780}^{2500} T(\lambda) d(\lambda)}{(2500-780)\times 100} \times 100\%$

[c] Average shielding ratio of near-infrared light region (780-2500nm): $S_{NIR} = 100\% - T_{NIR}$